Int. J. Electrochem. Sci., 6 **(2011)** 3093 - 3104

International Journal of
ELECTROCHEMICAL
SCIENCE
www.electrochemsci.org

Cycle Performance of Sn Electrode Electrodeposited in Different Conditions for Li-ion Batteries

Jung-Won Park[a], *Ji-Yong Eom*[b,*], *and Hyuk-Sang Kwon*[a,**]

[a]Department of Materials Science & Engineering, KAIST, 373-1, Guseong-dong, Yuseong-gu, Daejeon, 305-701, Korea
[b]Battery Development Team, Energy Business Division, Samsung SDI Co., Ltd., 508, Sungsung-dong, Cheonan, Chungcheongnam-do, 330-300, Korea
[*]E-mail: jyeom74@gmail.com
[**]E-mail: hskwon@kaist.ac.kr

Received: 7 April 2011 / *Accepted:* 2 July 2011 / *Published:* 1 August 2011

The effects of electrodeposition conditions on the cycle performance of Sn electrodes were investigated in this study. Sn electrodes were electrodeposited on Cu substrates under different conditions, such as the electrodeposition baths and the current densities to maximize cycle performance and coulombic efficiency. By using different types of electrodeposition baths, Sn electrodes with different phases were electrodeposited. The formation of an η-Cu_6Sn_5 phase between the Sn layer and Cu substrate contributes to the improvement of the cycle performance of the Sn electrode. As the current density increased, the Sn layers became less dense structure with nodule-type morphology. The less dense Sn electrodes with nodule-type morphology exhibited a better cycle performance due to the absence of the high-voltage irreversible reaction and their buffering effects for volume expansion.

Keywords: Sn; Electrodeposition; Anode; Cycle performance; Li-ion batteries

1. INTRODUCTION

Sn-based materials have been studied as an anode material for Li-ion batteries because of their higher Li storage capacity (991 mAh g^{-1}, the theoretical limit of $Li_{4.4}Sn$) [1-3]. However, a pure Sn electrode suffers severely from its poor cycle performance due to its abrupt volume expansion (up to approximately 300 %) during the charge/discharge process. To improve the cycle performance of Sn electrodes, several studies have suggested that both the size of the particles comprising the electrode and the size of the grains within these particles play critical roles in electrochemical performance [3-5]. Recently, Sn-based alloys, including Sn–Co [6,7], Sn–Ni [8,9], and Sn–Cu [10-13] have received

much attention for their improvement to the cycle performance of the Sn-based electrode. However, as the applied potential increases, the alloy structure is deformed, causing large volume expansion and poor cycle performance.

To overcome this problem, various approaches have been applied to the Sn-based electrode. Pu et. al. [13] reported that the cycle performance of Sn-Cu alloy electrode could be improved by coating of protective Cu layer on the surface of the electrode. The protective Cu layer restrained the pulverization of electrode during charge and discharge. Also, porous structural materials have been focused upon as promising new electrode materials for Li-ion batteries due to the following advantages: (i) large open pores that allow easily transport of liquid electrolyte, (ii) a high number of active sites for charge transfer reactions due to the high surface area of materials, (iii) the continuous network of pores that is expected to improve electrical conductivity, and (iv) numerous pores that can buffer the large volume change [14]. Although porous structural materials can be fabricated by various methods, an electrodeposition process has various advantages: (i) it is much simpler than the currently used powder process because neither a binder nor a conductive agent is required, (ii) a comparatively high initial coulombic efficiency and high conductivity can be expected, and (iii) the deposited structure can be easily adjusted by controlling the electrodeposition conditions, such as the chemical composition of electrodeposition baths, the bath temperature, and the current densities.

We have investigated the structure and cycle performance of Sn electrodes electrodeposited under different conditions, such as the electrodeposition baths and the current densities. This study has demonstrated that the cycle performance of electrodeposited Sn electrodes can be significantly improved by controlling the electrodeposition conditions.

2. EXPERIMENTAL

2.1. Electrodeposition of Sn electrodes

Sn electrodes were electrodeposited on 18 μm Cu substrates under different conditions, such as the electrodeposition baths and the current densities. Three compositions of the electrodeposition baths were used in this work (Table 1). To obtain Sn electrodes with different structure and morphology, the current densities in the pyrophosphate bath (Bath 1, Table 1) were increased from 10 to 40 and 50 mA cm^{-2}.

The Sn electrodeposition was performed galvanostatically in each bath after removal of a surface oxide film by soaking in a 100 g l^{-1} H_2SO_4 solution and subsequent rinsing with de-ionized water. After electrodeposition, each Sn electrode was cut to approximately 1 cm^2 and dried in a vacuum for 12 h.

2.2. Electrochemical test of Li/Sn cells

The Li/Sn cells were assembled using a 2016 coin-type cell in an argon-filled glove box. A polypropylene separator soaked with a liquid electrolyte (provided by Merck©), consisting of 1 M of

$LiPF_6$ dissolved in a 1:1 volume ratio of ethylene carbonate (EC) and dimethyl carbonate (DMC), was placed between the anode and the Li-cathode in the cell.

The charge/discharge test of the Li/Sn cells was performed in a galvanostatic mode using a TOSCAT 3000 (Toyo System©) system. The cells were charged (lithiation) and discharged (delithiation) at a constant current of 100 mA g^{-1} between 0.02 and 1.5 V.

3. RESULTS AND DISCUSSION

3.1. Structure and cycle performance of Sn electrodeposited in different baths

Figure 1 shows the cathodic polarization behaviors of Sn electrodeposited in each bath. In baths 1 and 2, the Sn nucleation was initiated around -1000 mV_{SCE}, with a current density of 0.1 mA cm^{-2}.

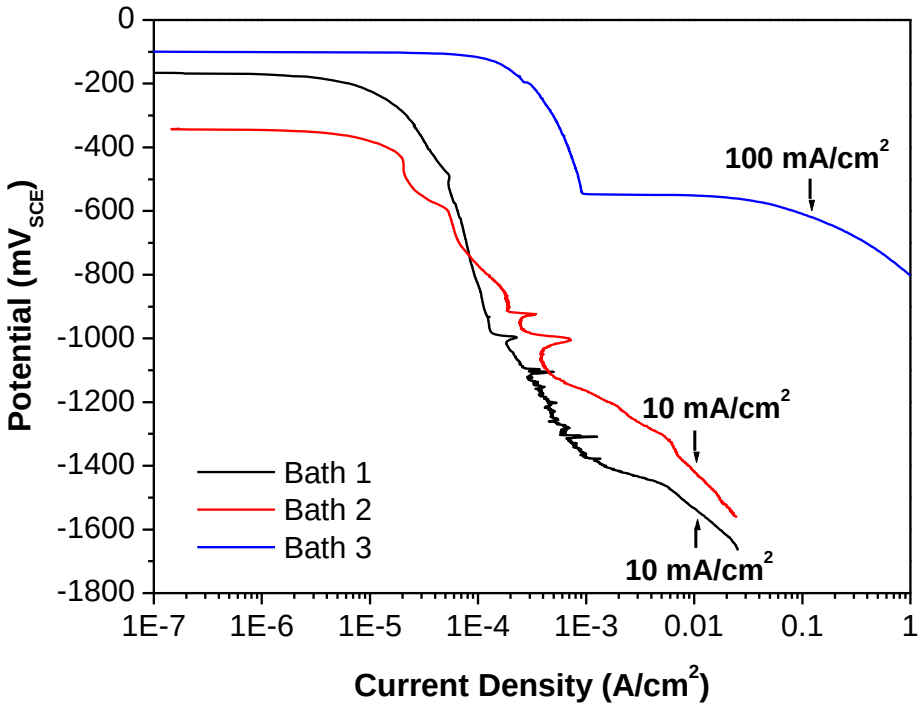

Figure 1. Cathodic polarization behaviors of Sn electrodeposited in each bath.

Thus, a current density of more than 0.1 mA cm^{-2} should be applied to nucleate the Sn. A uniform Sn layer was observed at 10 mA cm^{-2}. However, the cathodic polarization behavior of Sn prepared in bath 3 was different compared with those of baths 1 and 2, which was possibly due to the low pH. In bath 3, Sn nucleation initiated near -600 mV_{SCE}, and a uniform Sn layer was observed at 100 mA cm^{-2}. Figure 2 shows the loading density and thickness of Sn layers electrodeposited in each bath. In baths 1 and 2, Sn layers with 1 μm thickness were prepared when 10 mA cm^{-2} current density

was applied for 4 min and 1 min, respectively. Similar layers were produced in bath 3 when 100 mA cm^{-2} current density was applied for 12 sec.

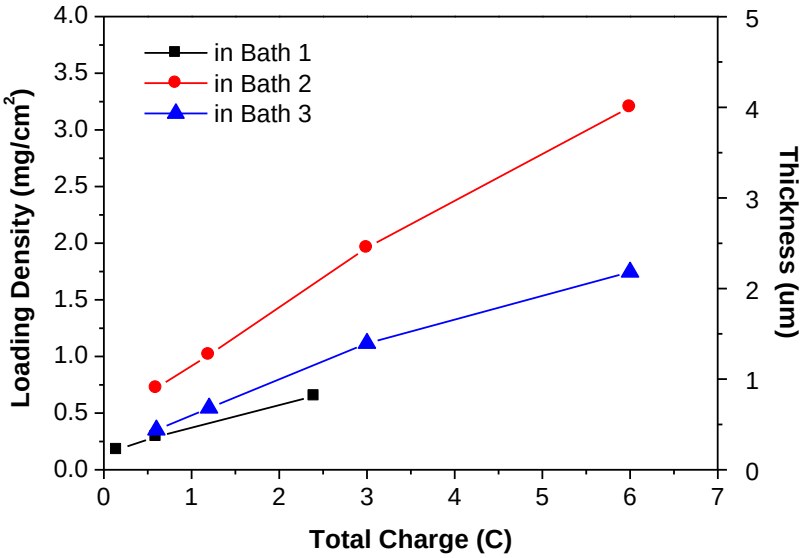

Figure 2. Loading density and thickness of Sn layers electrodeposited in each bath.

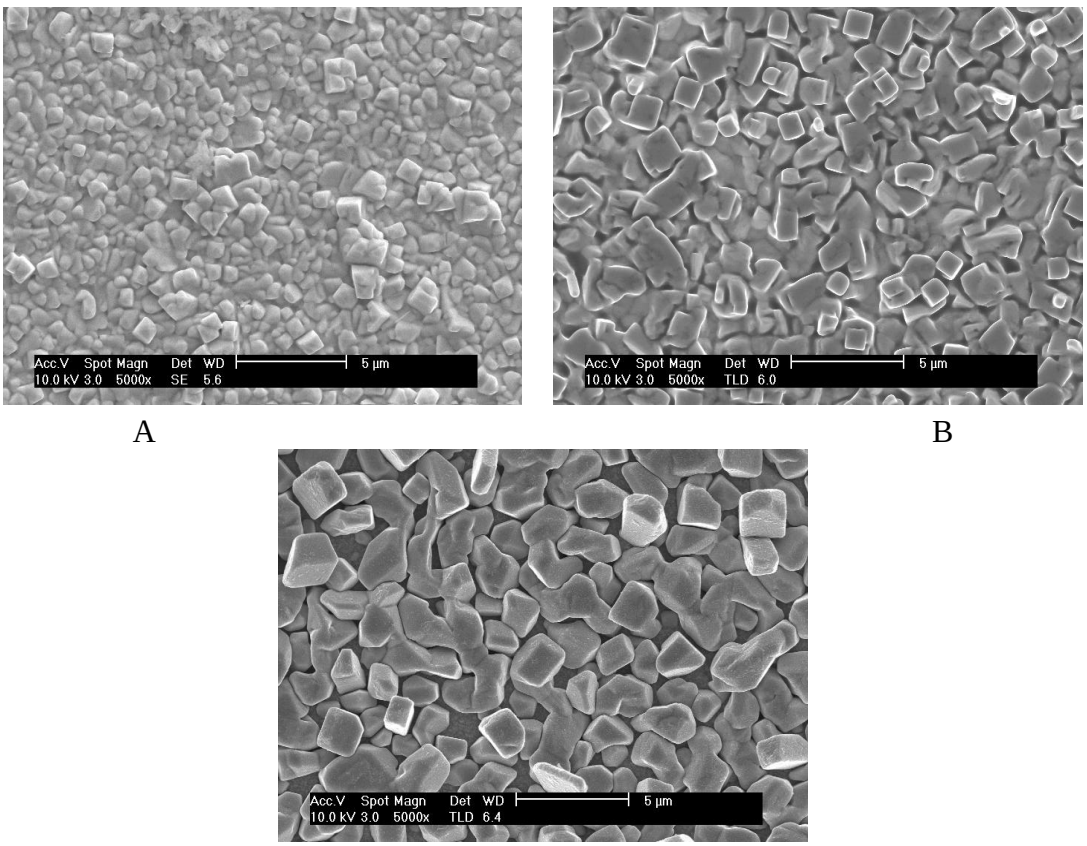

Figure 3. SEM images on the surface of Sn layers electrodeposited in each bath; (a) at 10 mA cm^{-2} for 4 min in bath 1, (b) at 10 mA cm^{-2} for 1 min in bath 2, and (c) at 100 mA cm^{-2} for 12 sec in bath 3.

Figure 3 shows the scanning electron microscopy (SEM) images on the surface of Sn layers electrodeposited in each bath, indicating that Sn layers with different crystal size grew. Smaller crystals of Sn should have better electrochemical performance than bigger ones [13]. X-ray diffraction (XRD) patterns of Sn layers with 1 μm thickness electrodeposited in each bath are shown in Figure 4.

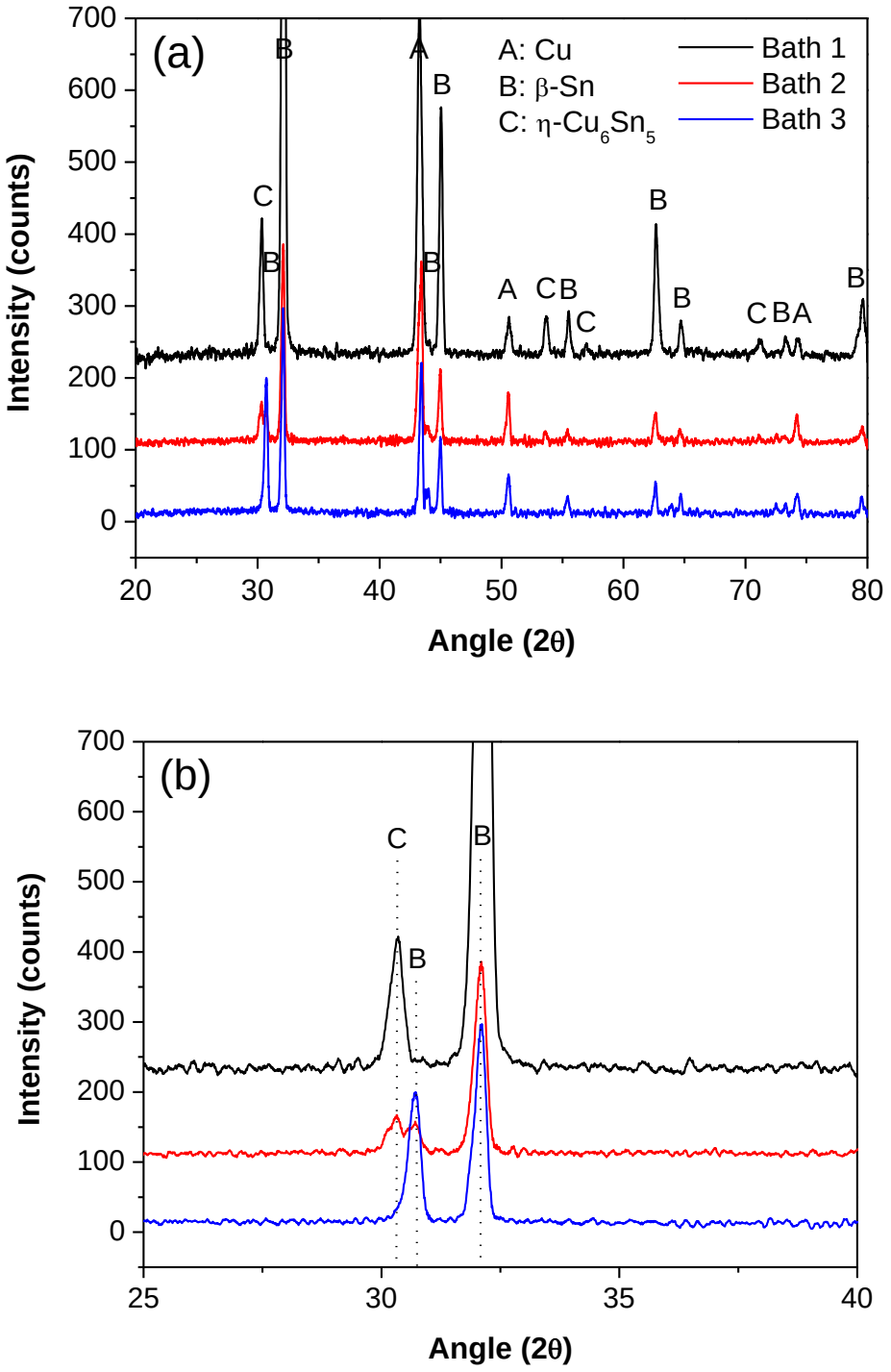

Figure 4. (a) XRD patterns of Sn layers electrodeposited in each bath and (b) enlarged patterns in the range of 25 ~ 40 ° in 2θ.

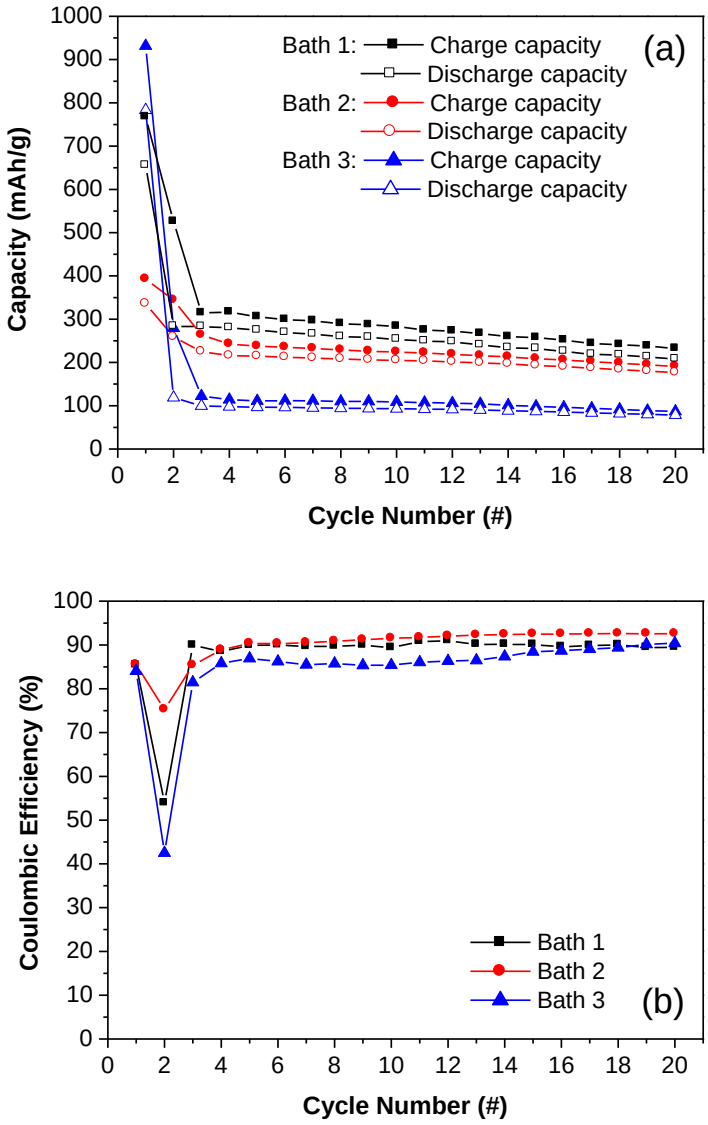

Figure 5. (a) Cycle performance and (b) coulombic efficiency of the Sn electrodes electrodeposited in each bath.

In the patterns of Sn layers prepared in baths 1 and 2, peaks of Cu substrate, electrodeposited β-Sn, and a small amount of η-Cu_6Sn_5 were observed. In the Sn layer prepared in bath 1, more η-Cu_6Sn_5 was formed than in bath 2. To contrast, the peaks of η-Cu_6Sn_5 were not observed in the XRD pattern of Sn layer prepared in bath 3. The Sn electrodes prepared in baths 1 and 2 included a thin η-Cu_6Sn_5 phase between the electrodeposited β-Sn layer and Cu substrate.

Figure 5 shows the cycle performance and the coulombic efficiency of the Sn electrodes electrodeposited in each bath. In the first cycle, the C_{rev} of the Sn electrode produced from bath 3 (783 mAh g^{-1}) was higher than that of the Sn electrodes from bath 1 (656 mAh g^{-1}) and bath 2 (336 mAh g^{-1}). However, the C_{irr} of the electrode from bath 3 (149 mAh g^{-1}) was higher than that of the Sn electrodes from bath 1 (112 mAh g^{-1}) and bath 2 (57 mAh g^{-1}). Therefore, the coulombic efficiency of electrode from bath 3 (84 %) was lower than that of electrodes from bath 1 (85 %) and 2 (85 %). This

lack of efficiency showed that the Sn electrode prepared in bath 3 was composed only of Sn without an η-Cu_6Sn_5 phase, as presented in the XRD results (Figure 4). Although pure Sn has a higher Li storage capacity, it presents higher C_{irr} and poorer cycle performance due to its large volume expansion. To compare the electrodes from baths 1 and 2, the Sn content of electrode from bath 1 was higher than that of electrode from bath 2, relatively. Therefore, although the C_{rev} of the electrode from bath 1 was higher than that of electrode from bath 2, the C_{irr} of the bath 1 electrode was also higher in the first cycle. Previous studies showed that the formation of an η-Cu_6Sn_5 phase between the electrodeposited Sn layer and Cu substrate contributes to improve the cycle performance of the Sn electrode [15]. Therefore, the cycle performance of the electrodes in baths 1 and 2 with η-Cu_6Sn_5 phases was better than that of the electrode in bath 3. In addition, the coulombic efficiency in the second cycle decreases in conjunction with higher Sn content, caused by a strange phenomenon called 'high-voltage irreversible capacity', which appears in electrodes of higher Sn content during the second charge process [16].

3.2. Structure and cycle performance of Sn electrodeposited in different current densities

The morphology of the electrodeposited layer at high current density is transformed from more dense to less dense structure. Sn electrodes were electrodeposited with 10, 40, and 50 mA cm^{-2} current densities in bath 1 (Table 1), and labeled as P0, P1, and P2, respectively.

Table 1. The electrodeposition baths used in this work.

Bath 1	**Pyrophosphate**	**30 g l^{-1} $Sn_2P_2O_7$ + 120 g l^{-1} $K_4P_2O_7$ + 0.15 g l^{-1} Gelatine**
Bath 2	Chloride dihydrate	23 g l^{-1} $SnCl_2{\cdot}2H_2O$ + 165 g l^{-1} $K_4P_2O_7$ + 30 g l^{-1} Glycine
Bath 3	Sulfate	40 g l^{-1} $SnSO_4$ + 150 g l^{-1} H_2SO_4 + 5 g l^{-1} Formalin

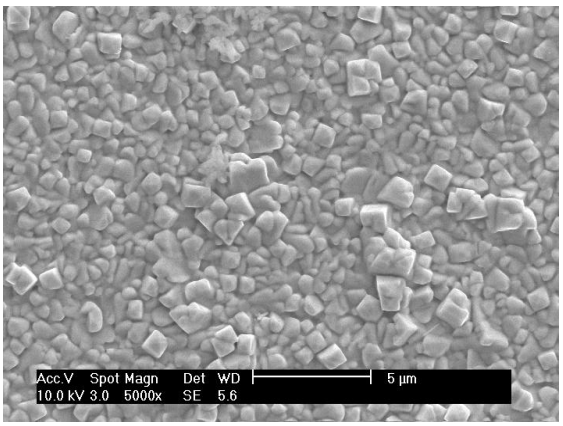

A

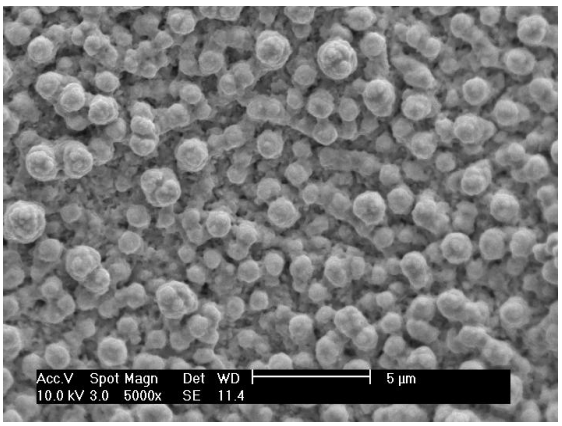

B

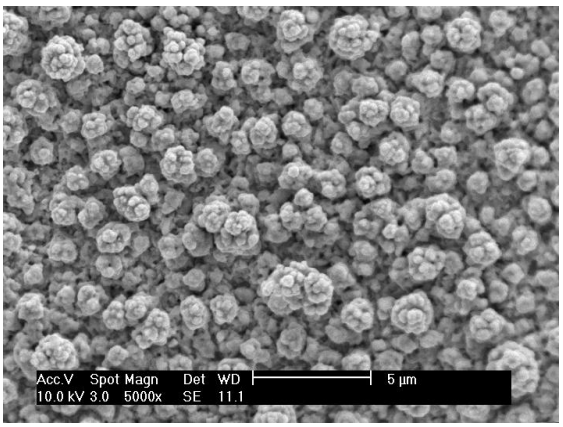

C

Figure 6. SEM images on the surface of the Sn layers electrodeposited at (a) 10, (b) 40, and (c) 50 mA cm^{-2} in bath 1.

Figure 6 shows the SEM images of the surface of the Sn layers electrodeposited at each current density. As the current density increased, the electrodeposited Sn layers became less dense structure with nodule-type morphology, which was due to more nucleation sites created by high overpotential when the high current was applied.

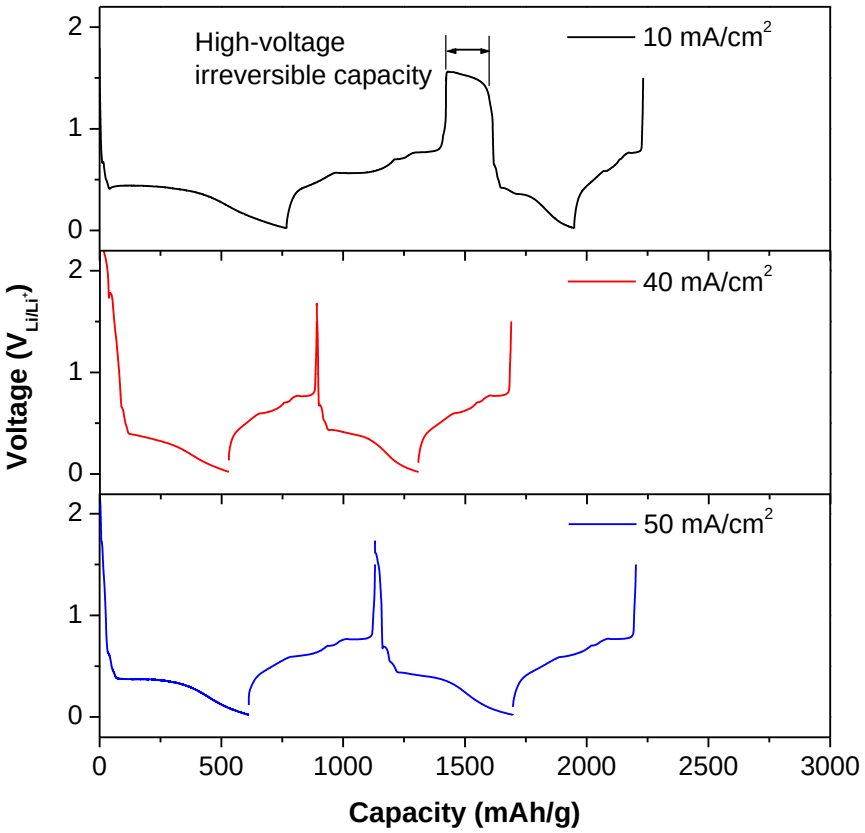

Figure 7. Charge/discharge curves in the first and second cycles of the Sn electrodes electrodeposited at each current density; 10, 40, and 50 mA cm^{-2} in bath 1.

The charge/discharge curves in the first and second cycles of the Sn electrodes electrodeposited at each current density are shown in Figure 7. In the first cycle, the C_{rev} of the P0 electrode was higher than that of the P1 and P2 electrodes, and the C_{irr} of the P0 electrode was lower than that of the P1 and P2 electrodes. However, in the second cycle, the C_{rev} of the P0 electrode abruptly decreased and was lower than that of the P1 and P2 electrodes, because a 'high-voltage irreversible capacity' phenomenon appeared during charge process in the P0 electrode.

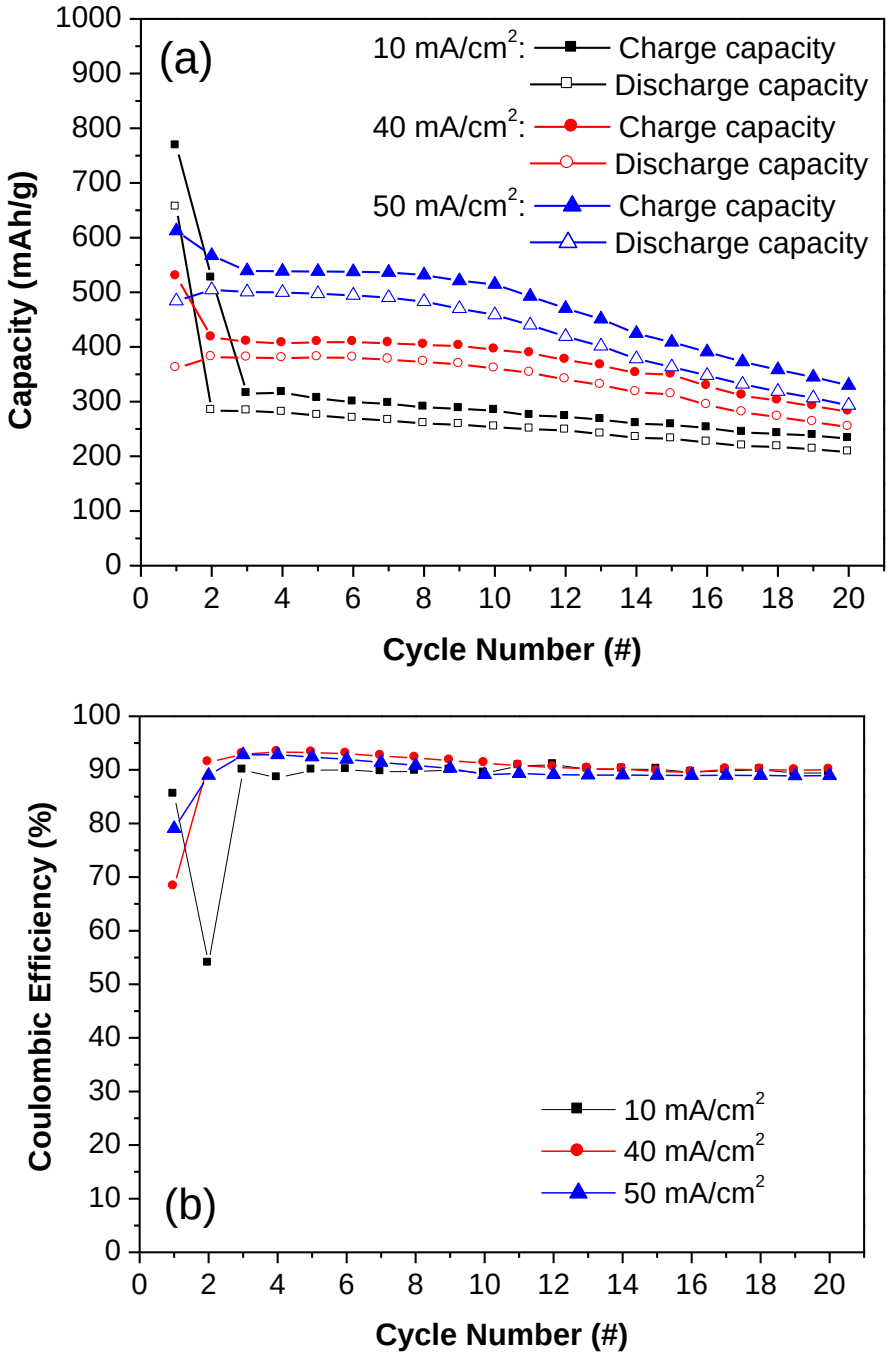

Figure 8. (a) Cycle performance and (b) coulombic efficiency of the Sn electrodes electrodeposited at each current density; 10, 40, and 50 mA cm^{-2} in bath 1.

This phenomenon occurs during the charging process of the Sn anode at a high voltage region over 1 V due to the formation of a new layer caused by electrolyte decomposition at the catalytic Sn surface, which is increased by the cracking of the Sn electrode due to abrupt volume expansion during the first cycle [16]. The high-voltage irreversible reaction causes a large amount of irreversible capacity, and finally significantly lowers the cycle performance of the Sn anode. Therefore, it is expected that the P1 and P2 electrodes without the high-voltage irreversible capacity exhibit better cycle performance than the P0 electrode.

Figure 8 shows the cycle performance and the coulombic efficiency of the Sn electrodes electrodeposited at each current density. In the first cycle, although the C_{rev} and the coulombic efficiency of the P0 electrode (656 mAh g^{-1}, 85 %) was higher than those of the P1 (361 mAh g^{-1}, 68 %) and P2 (484 mAh g^{-1}, 79 %) electrodes, those of the P0 electrode abruptly decreased in the second cycle due to the high-voltage irreversible capacity. After the 20th cycle, the C_{rev} of the P2 electrode (293 mAh g^{-1}) was higher than that of P0 (208 mAh g^{-1}) and P1 (254 mAh g^{-1}) electrodes.

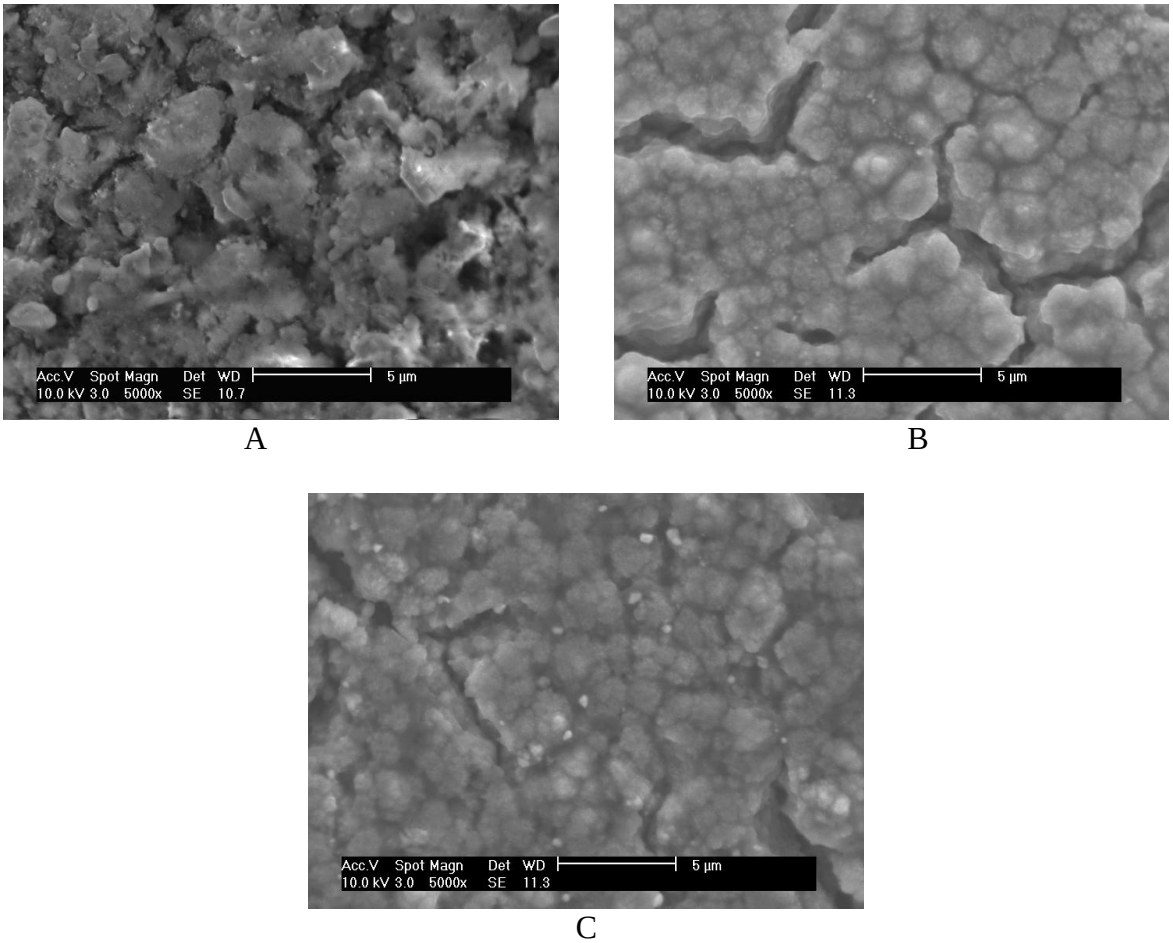

A B C

Figure 9. SEM images on the surface of the Sn electrodes electrodeposited at each current density; (a) 10, (b) 40, and (c) 50 mA cm^{-2} in bath 1 after the 20th cycle.

This degradation of C_{rev} in P0 and P1 demonstrates that the Sn electrodes of less dense

structure with nodule-type morphology presented better cycle performance without showing high-voltage irreversible capacity. To examine the causes of higher C_{rev} for the less dense Sn electrode, the surface morphology of the Sn electrodes electrodeposited at each current density after the 20^{th} cycle were observed by SEM, as shown in Figure 9. As the current density increased, a less amount of cracking was observed on the surface of the Sn electrodes after the 20^{th} cycle. This demonstrates that less mechanical stress was applied to the P1 and P2 electrodes than to the P0 electrode due to their less dense structure. In addition, when the P1 and P2 electrodes were compared, the P2 electrode suffered from less mechanical stress as confirmed by less cracking seen in the SEM images. Therefore, the less dense Sn electrodes with nodule-type morphology exhibited a better cycle performance due to the absence of the high-voltage irreversible reaction and their buffering effects for volume expansion.

4. CONCLUSIONS

By altering the chemical composition of the electrodeposition baths, Sn electrodes with different phases were electrodeposited. The Sn electrodes prepared in baths containing pyrophosphate (bath 1) and chloride dihydrate (bath 2) were composed mostly of a β-Sn and thin η-Cu_6Sn_5 phase. However, the Sn electrode prepared in the sulfate (bath 3) bath was composed only of a β-Sn phase. The cycle performance of the electrodes from bath 1 and 2 with an η-Cu_6Sn_5 phase was better than that of the electrode from bath 3.

The structure of Sn electrodes prepared in bath 1 became less dense with nodule-type morphology when the current density was increased. The more dense Sn electrodes exhibited the high-voltage irreversible capacity phenomenon during charge process due to the cracking of the Sn electrode caused by abrupt volume expansion. The high-voltage irreversible reaction causes a large amount of irreversible capacity, and finally significantly lowers the cycle performance of the Sn anode. Therefore, the less dense Sn electrodes with nodule-type morphology exhibited a better cycle performance due to the absence of the high-voltage irreversible reaction and their buffering effects for volume expansion.

Acknowledgements

This work was supported by the Growth Engine Technology Development Program (Project No. 10016472) and the BK21 Program funded by Korea Ministry of Knowledge Economy.

References

1. Y. Idota, T. Kubota, A. Matsufuji, Y. Maekawa, T. Miyasaka, *Science* 276 (1997) 1395.
2. I.A. Courtney, J.R. Dahn, *J. Electrochem. Soc.* 144 (1997) 2045.
3. J.O. Besenhard, J. Yang, M. Winter, *J. Power Sources* 68 (1997) 87.
4. I.A. Courtney, J.R. Dahn, *J. Electrochem. Soc.* 144 (1997) 2943.
5. N. Li, C.R. Martin, *J. Electrochem. Soc.* 148 (2001) A164.

6. N. Tamura, M. Fujimoto, M. Kamino, S. Fujitani, *Electrochim. Acta* 49 (2004) 1949.
7. J.J. Zhang, Y.Y. Xia, *J. Electrochem. Soc*. 153 (2006) A1466.
8. H. Mukaibo, T. Sumi, T. Yokoshima, T. Momma, T. Osaka, *Electrochem. SolidState Lett*. 6 (2003) A218.
9. [9] F.S. Ke, L. Huang, H.H. Jiang, H.B. Wei, F.Z. Yang, S.G. Sun, *Electrochem. Commun*. 9 (2007) 228.
10. N. Tamura, R. Ohshita, M. Fujimoto, S. Fujitani, M. Kamino, I. Yonezu, *J. Power Sources* 107 (2002) 48.
11. S.D. Beattie, J.R. Dahn, *J. Electrochem. Soc*. 150 (2003) A894.
12. F.S. Ke, L. Huang, J.S. Cai, S.G. Sun, *Electrochimica Acta* 52 (2007) 6741.
13. W. Pu, X. He, J. Ren, C. Wan, C. Jiang, *Electrochimica Acta* 50 (2005) 4140.
14. H. Yan, S. Sokolov, J.C. Lytle, A. Stein, F. Zhang, W.H. Smyrl, *J. Electrochem. Soc.* 150 (2003) A1102.
15. J.W. Park, S. Rajendran, H.S. Kwon, *J. Power Sources* 159 (2006) 1409.
16. S.D. Beattie, T. Hatchard, A. Bonakdarpour, K.C. Hewitt, J.R. Dahn, *J. Electrochem. Soc*. 150 (2003) A701.